Tsunami Dynamics

2

2.1 Introduction

The approach of a tsunami wave towards shore can be an awesome sight to those who have witnessed it and survived. Figure 2.1 represents an artist's impression of a tsunami wave approaching the coast of Unimak Island, Alaska, early on April 1, 1946. Similar artists' impressions of breaking tsunami will be presented throughout this text. The impressions are accurate. Whereas ordinary storm waves or swells break and dissipate most of their energy in a surf zone, tsunami break at, or surge over, the shoreline. Hence, they lose little energy as they approach a coast and can run up to heights an order of magnitude greater than storm waves. Much of this behavior relates to the fact that tsunami are very long waves—kilometers in length. As shown in Fig. 2.1, this behavior also relates to the unusual shape of tsunami wave crests as they approach shore. This chapter describes these unique features of tsunami.

2.2 Tsunami Characteristics

Tsunami characteristics are described by many authors (Wiegel 1964; Bolt et al. 1975; Shepard 1977; Myles 1985). The terminology used in this text for tsunami waves is shown schematically in Fig. 2.2. Much of this terminology is the same as that used for ordinary wind waves. Tsunami have a wavelength, a period, and a deep-water or open-ocean height. They can undergo shoaling, refraction, reflection and diffraction (Murata et al. 2010). Most tsunami generated by large earthquakes travel in wave trains containing several large waves that in deep water are less than 0.4 m in height. Figure 2.3 plots typical tidal gauge records or *marigrams* of tsunami at various locations in the Pacific Ocean (Wiegel 1970). These records are taken close to shore and show that tsunami wave heights increase substantially into shallow water. Tsunami wave characteristics are highly variable. In some cases, the waves in a tsunami wave train consist of an initial peak that then tapers off in height exponentially over four to 6 h. In other cases, the tsunami wave train consists of a maximum wave peak well back in the wave sequence. The time it takes for a pair of wave crests to pass by a point is termed the wave period. This is a crucial parameter in defining the nature of any wave. Tsunami typically have periods of 100–2,000 s (1.6–33 min), referred to as the *tsunami window*. Waves with this period travel at speeds of 600–900 km hr^{-1} (166–250 m s^{-1}) in the deepest part of the ocean, 100 –300 km hr^{-1} (28–83 m s^{-1}) across the continental shelf, and 36 km hr^{-1} (10 m s^{-1}) at shore (Iida and Iwasaki 1983). The upper limit is the speed of a commercial jet airplane. Because of the finite depth of the ocean and the mechanics of wave generation by earthquakes, a tsunami's wavelength—the distance between successive wave crests—lies between 10 and 500 km. These long wavelengths make tsunami profoundly different from swell or storm waves.

Tsunami waves can have different shapes depending upon where they are placed with respect to the shore and the depth of water (Geist 1997). The simplest form of ocean waves is sinusoidal in shape and oscillatory (Fig. 2.4). Water particles under oscillatory waves transcribe closed orbits. Hence there is no mass transport of water shoreward with the passage of the wave. Oscillatory waves are described for convenience by three parameters: their height or elevation above the free water surface, their wavelength, and water depth (Fig. 2.2). These parameters can be related to each other by three ratios as follows (Komar 1998):

$$H : L, H : d, L : d \tag{2.1}$$

where

H = crest-to-trough wave height (m)
L = wavelength (m)
d = water depth (m)

E. Bryant, *Tsunami*, DOI: 10.1007/978-3-319-06133-7_2,

Fig. 2.1 An artist's impression of the tsunami of April 1, 1946 approaching the five story-high Scotch Cap lighthouse, Unimak island, Alaska. The lighthouse, which was 28 m high, stood on top of a bluff 10 m above sea level. It was completely destroyed (see also Fig. 2.8). The wave ran over a cliff 32 m high behind the lighthouse. Painting is by Danell Millsap, commissioned by the United States National Weather Service

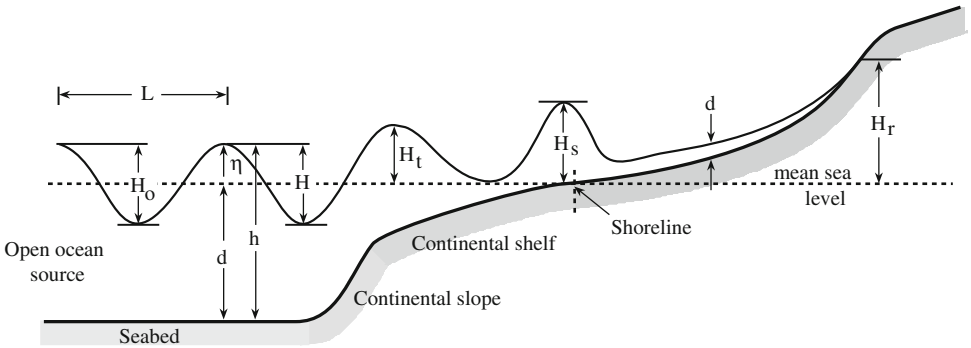

Fig. 2.2 Various terms used in the text to express the wave height of a tsunami

In deep water, the most significant factor is the ratio *H*:*L*, or wave steepness. In shallow water it is the ratio *H*:*d*, or relative height. Sinusoidal waves fit within a class of waves called cnoidal waves: c for cosine, n for an integer to label the sequence of waves, and *oidal* to show that they are sinusoidal in shape. The shape of a wave or its peakedness can be characterized by a numerical parameter. For sinusoidal waves this parameter is zero. While tsunami in the open ocean are approximately sinusoidal in shape, they become more peaked as they cross the continental shelf. In this case, the numerical parameter describing shape increases and non-linear terms become important. The wave peak sharpens while the trough flattens. These non-linear, tepee-shaped waves are characterized mathematically by Stokes wave theory (Komar 1998; von Baeyer 1999). In Stokes theory, motion in two dimensions is described by the sum of two sinusoidal components (Fig. 2.4). Water particles in a Stokes wave do not follow closed orbits, and there is mass movement of water throughout the water column as the wave passes by a point. As a tsunami wave approaches shore, the separation between the wave crests becomes so large that the trough disappears and only one peak remains. The numerical parameter characterizing shape approaches one and the tsunami wave becomes a solitary wave (Fig. 2.4). Solitary waves are translatory in that water moves with the crest. All of the waveform also lies above mean sea level. Finally, it has been noted that a trough that is nearly as deep as the crest is high precedes many exceptional tsunami waves. This gives the incoming wave a wall effect. The Great Wave of Kanagawa shown on the frontispiece of this book is of this type. These waves are not solitary because they have a component below mean sea level. Such waveforms are better characterized by *N*-waves. This chapter uses features of each of these wave types: sinusoidal, Stokes, solitary, and *N*-waves to characterize tsunami.

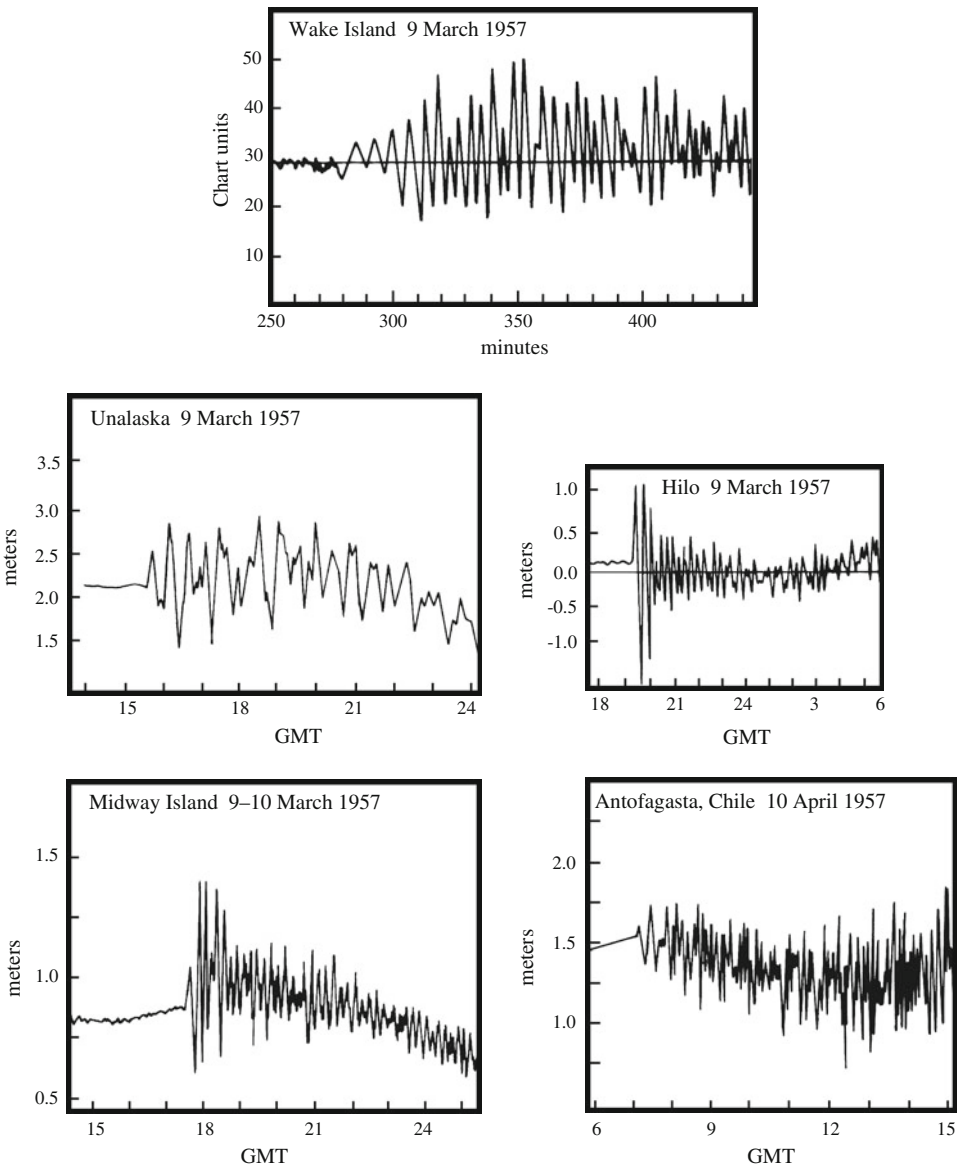

Fig. 2.3 Plots or marigrams of tsunami wave trains at various tidal gauges in the Pacific region. Based on Wiegel (1970)

2.3 Tsunami Wave Theory

The theory of waves, and especially tsunami waves, are described in many basic references (Wiegel 1964, 1970; Pelinovsky 1996; Geist 1997; Trenhaile 1997; Komar 1998). The simplest form describing any wave is that represented by a sine curve (Fig. 2.4). These sinusoidal waves and their features can be characterized mathematically by linear, trigonometric functions known as Airy wave theory (Komar 1998). This theory can represent local tsunami propagation in water depths greater than 50 m. In this theory, the three ratios presented in Eq. 2.1 are much less than one. This implies that wave height relative to wavelength is very low—a feature characterizing tsunami in the open ocean. The formulae describing sinusoidal waves vary depending upon the wave being in deep or shallow water. Shallow water begins when the depth of water is less than half the wavelength. As oceans are rarely more than 5 km deep, the majority of tsunami travel as shallow-water waves. In this case, the trigonometric functions characterizing sinusoidal waves disappear and the velocity of the wave becomes a simple function of depth as follows:

$$C = (gd)^{0.5} \tag{2.2}$$

where

C = wave speed (m s^{-1})
g = gravitational acceleration (9.81 m s^{-1})

The wavelength of a tsunami is also a simple function of wave speed, C, and period, T, as follows:

$$L = CT \tag{2.3}$$

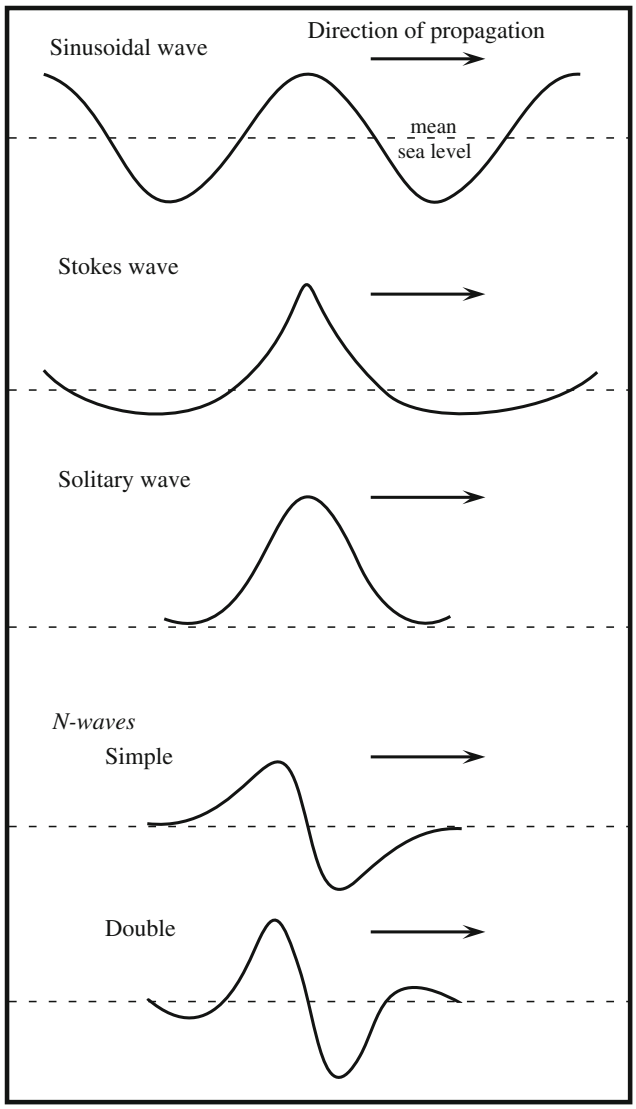

Fig. 2.4 Idealized forms characterizing the cross-section of a tsunami wave. Based on Geist (1997). Note that the vertical dimension is greatly exaggerated

Equation 2.3 holds for linear, sinusoidal waves and is not appropriate for calculating the wavelength of a tsunami as it moves into shallow water. Linear theory can be used as a first approximation to calculate changes in tsunami wave height as the wave moves across an ocean and undergoes wave shoaling and refraction. The following formulae apply:

$$H = K_r K_s H_o \tag{2.4}$$

$$K_r = \left(b_o b_i^{-1}\right)^{0.5} \tag{2.5}$$

$$K_s = \left(d_o d_i^{-1}\right)^{0.25} \tag{2.6}$$

where

H_o = crest-to-trough wave height at the source point (m)
K_r = refraction coefficient (dimensionless)
K_s = shoaling coefficient (dimensionless) (Green's Law)
b_o = distance between wave orthogonals at a source point water (m)
b_i = distance between wave orthogonals at any shoreward point (m)
d_o = water depth at a source point (m)
d_i = water depth at any shoreward point (m)

Note that there is a plethora of definitions of wave height in the tsunami literature. These include wave height at the source region, wave height above mean water level, wave height at shore, and wave run-up height above present sea level. The distinctions between these expressions are presented in Fig. 2.2. The expression for shoaling—Eq. 2.6—is known as Green's Law (Geist 1997). For example, if a tsunami with an initial height of 0.6 m is generated in a water depth of 4000 m, then its height in 10 m depth of water on some distant shore can be raised 4.5 times to 2.7 m. Because tsunami are shallow-water waves, they *feel* the ocean bottom at any depth and their crests undergo refraction or bending around higher seabed topography. The degree of refraction can be measured by constructing a set of equally spaced lines perpendicular to the wave crest. These lines are called wave orthogonals or rays (Fig. 2.5). As the wave crest bends around topography, the distance, b, between any two lines will change. Refraction is measured by the ratio b_o:b_i. Simple geometry indicates that the ratio b_o:b_i is equivalent to the ratio $\cos\alpha_o$:$\cos\alpha_i$, where α is the angle that the tsunami wave crest makes to the bottom contours as the wave travels shoreward (Fig. 2.5). Once this angle is known, it is possible to determine the angle at any other location using Snell's Law as follows:

$$\sin\alpha_o C_o^{-1} = \sin\alpha_i C_i^{-1} \tag{2.7}$$

where

α_o = the angle a wave crest makes to the bottom contours at a source point (degrees)
α_i = the angle a wave crest makes to the bottom contours at any shoreward point (degrees)
C_o = wave speed at a source point (m s^{-1})
C_i = wave speed at any shoreward point (m s^{-1})

For a tsunami wave traveling from a distant source—such as occurs often in the Pacific Ocean—the wave path or ray must also be corrected for geometrical spreading on a spherical surface (Okal 1988). Equation 2.4 can be rewritten to incorporate this spreading as follows:

$$H = K_r K_s K_{sp} H_o \tag{2.8}$$

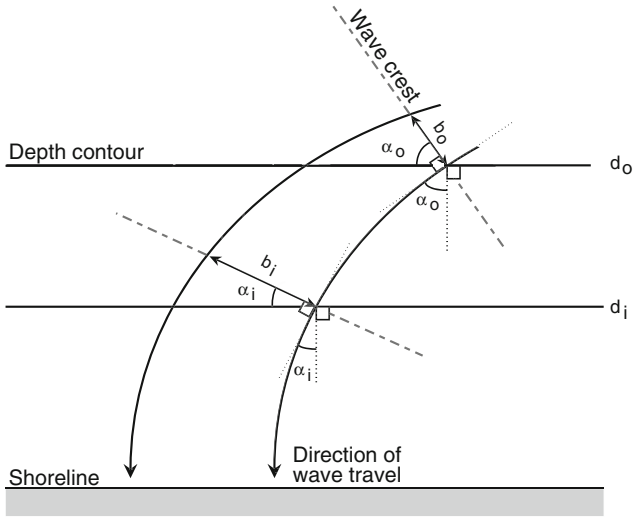

Fig. 2.5 Refraction of a tsunami wave crest as it approaches shore

where

K_{sp} = $(\sin \Delta)^{-0.5}$
K_{sp} = coefficient of geometrical spreading on a sphere (dimensionless)
Δ = angle of spreading on a sphere relative to a wave's direction of travel

In a large ocean, bathymetric obstacles such as island chains, rises, and seamounts can refract a tsunami wave such that its energy is concentrated or *focused* upon a distant shoreline (Okal 1988). These are known as *teleseismic* tsunami because the effect of the tsunami is translated long distances across an ocean. Japan is particularly prone to tsunami originating from the west coast of the Americas, despite this coastline laying half a hemisphere away. On the other hand, bottom topography can spread tsunami wave crests, dispersing wave energy over a larger area. This process is called *defocussing*. Tahiti, but not necessarily other parts of French Polynesia, is protected from large tsunami generated around the Pacific Rim because of this latter process.

Headlands are particularly prone to the amplification of tsunami height due to refraction However, this does not mean that bays are protected from tsunami. Reflection becomes a significant process for long waves such as tsunami that do not break at shore as wind waves do (Murata et al. 2010). The tsunami wave is reflected from the sides of an embayment towards shore. At shore, the wave is reflected seawards, then bent back to shore by refraction. This traps and concentrates the energy of tsunami waves along a bay's shoreline increasing the amplitude of succeeding waves. Trapping by this process can also occur around islands. This was particularly significant during the December 12, 1992 tsunami along the north coast of Flores Island, Indonesia, when the tsunami wrapped around Babi Island causing significant destruction on the lee side (Yeh et al. 1994). It also occurred on the south and west coasts of Sri Lanka during the Indian Ocean Tsunami of 2004. Finally, diffraction allows tsunami waves to bend around shielding land such as long headlands or islands more than 0.5 km in length.

Not all tsunami behave as sinusoidal waves. Many observations of tsunami approaching shore note that water is drawn down before the wave crest arrives. This characteristic can be due to non-linear effects that produce a trough in front of the wave. Solitons or *N*-waves mimic these features (Fig. 2.4) (Geist 1997; Tadepalli and Synolakis 1994). These type of waves will be discussed further when run-up is described.

2.3.1 Resonance

Tsunami, having long periods of 100–2,000 s, can also be excited or amplified in height within harbors and bays if their period approximates some harmonic of the natural frequency of the basin—termed resonance (Wiegel 1964, 1970). The word *tsunami* in Japanese literally means *harbor wave* because of this phenomenon. Here tsunami can oscillate back and forth for 24 h or more. The oscillations are termed *seiches,* a German word used to describe long, atmospherically induced waves in Swiss alpine lakes. Seiches are independent of the forcing mechanism and are related simply to the 3-dimensional form of the bay or harbor as follows:

$$\text{Closed basin}: T_s = 2L_b(gd)^{-0.5} \tag{2.9}$$

$$\text{Open basin}: T_s = 4L_b(gd)^{-0.5} \tag{2.10}$$

where

L_b = length of a basin or harbor (m)
T_s = wave period of seiching in a bay, basin, or harbor(s)

Equation 2.9 is appropriate for enclosed basins and is known as Merian's Formula. In this case, the forcing mechanism need have no link to the open ocean. As an example, an Olympic-sized swimming pool measuring 50 m long and 2 m deep would have a natural resonance period of 22.6 s. Any vibration with a periodicity of 5.6, 11.3, and 22.6 s could induce water motion back and forth along the length of the pool. If sustained, the oscillations or seiching would increase in amplitude and water could spill out of the pool. Seismic waves from earthquakes can provide the energy for seiching in swimming pools, and the Northridge earthquake of January 17, 1994 was very effective at emptying pools in Los Angeles (Bryant 2005).

Seiching was also induced in bays in Texas and the Great Lakes of North America about 30 min after the Great Alaskan Earthquake of 1964. Volcano-induced, atmospheric pressure waves can generate seiching as well. The eruption of Krakatau in 1883 produced a 0.5 m high seiche in Lake Taupo in the middle of the North Island of New Zealand via this process (Choi et al. 2003). Whether or not either of these phenomena technically is a tsunami is a moot point.

Resonance can also occur in any semi-enclosed body of water with the forcing mechanism being a sudden change in barometric pressure, semi- or diurnal tides, and tsunami. In these cases, the wave period of the forcing mechanism determines whether the semi-enclosed body of water will undergo excitation. The effects can be quite dramatic. For example, the predominant wave period of the tsunami that hit Hawaii on April 1, 1946 was 15 min. The tsunami was most devastating around Hilo Bay, which has a critical resonant length of about 30 min. While most tsunami usually approach a coastline parallel to shore, those in Hilo Bay often run obliquely alongshore because of resonance and edge-wave formation. Damage in Hilo due to tsunami has always been a combination of the tsunami and a tsunami-generated seiche. The above treatment of resonance is cursory. Harbor widths can also affect seiching and it is possible to generate subharmonics of the main resonant period that can complicate tsunami behavior in any harbor or bay. These aspects are beyond the scope of this text.

2.4 Modeling Tsunami

The preceding theories model either small amplitude or long waves. They cannot do both at same time. Tsunami behave as small amplitude, long waves. Their height-to-length ratio may be smaller than 1:100,000. If tsunami are modeled simply as long waves, they become too steep as they shoal towards shore and break too early. This is called the long-wave paradox. About 75 % of tsunami do not break during run-up. Because their relative height is so low, tsunami are also very shallow waves. Under these conditions, tsunami characteristics can be modeled more realistically by using non-linear, non-dispersive, shallow-water approximations of the Navier-Stokes equations (Liu et al. 2008). The description of these equations is beyond the scope of this book.

These equations work well in the open ocean, on continent slopes, around islands, and in harbors (Mader 1974, 1988). On a steep continental slope greater than 4°, the techniques show that a tsunami wave will be amplified by a factor of three to four times. Because they incorporate both flooding and frictional dissipation, the equations overcome problems with linear theory where the wave breaks too far from shore. They also show that, because of reflection, the second and third waves in a tsunami wave train can be amplified as the first wave in the train interacts with shelf topography. If shallow-water long-wave equations include vertical velocity components, they can describe wave motion resulting from the formation of cavities in the ocean surface (asteroid impacts); replicate wave profiles generated by sea floor displacement, underwater landslides, or tsunami traveling over submerged barriers; or simulate the behavior of short-wavelength tsunami. Effectively, an underwater barrier does not become significant in attenuating the tsunami wave height until the barrier height is more than 50 % the water depth. Even where the height of this barrier is 90 % of the water depth, half of the tsunami wave height can be transmitted across it. Modeling using the full shallow-water, long-wave equations shows that submerged offshore reefs do not necessarily protect a coast from the effects of tsunami. This is important because it indicates that a barrier such as the Great Barrier Reef of Australia may not protect the mainland coast from tsunami.

Shallow-water, long-wave approximations are solved using finite-difference techniques. Early models such as the SWAN code used simple, regularly spaced grids of ocean depths that incorporated Coriolis force and frictional effects (Mader 1988). To overcome the loss of detail as water shallowed, depth grids of increasing resolution were nested within each other. These models have given way to more advanced ones (Synolakis et al. 2008), which use triangular (3-point) or polygonal (4- or more point) grid cells that become smaller as bathymetry becomes more complex or coastlines more irregular. This matches the quality of most bathymetric data, which becomes more detailed towards shore. For example, the Indian Ocean Tsunami event on December 26, 2004 was modeled for the Banda Aceh region of Indonesia using a triangular grid that started out at a resolution of 14 km in the deep Indian Ocean, decreasing to 500 m near the coast and, finally, to 40 m at shore to model inundation throughout the city (Fig. 2.6) (Harig et al. 2008). Several advanced models are presently in use, including MOST (Tito and Gonzalez 1997), TUNAMI-N2/TUNAMI-N3 (Imamura et al. 2006) and SELFE (Zhang and Baptista 2008). The purpose of these models is to simulate accurately tsunami evolution, its propagation across an ocean to a coastline, its arrival time at shore and the limit of inundation on dry land. The MOST (Method of Splitting Tsunami) model can simulate all these components. An example of its use is shown in Fig. 2.7 for the height of the Tōhoku Tsunami of March 11, 2011 as it propagated into the Pacific Ocean from its source region on the east coast of Japan. While the effect of the tsunami was significant on the coast of Japan, this figure shows that there was minimal risk to coastlines outside the immediate area. By pre-computing hundreds of tsunami from possible earthquake scenarios, it

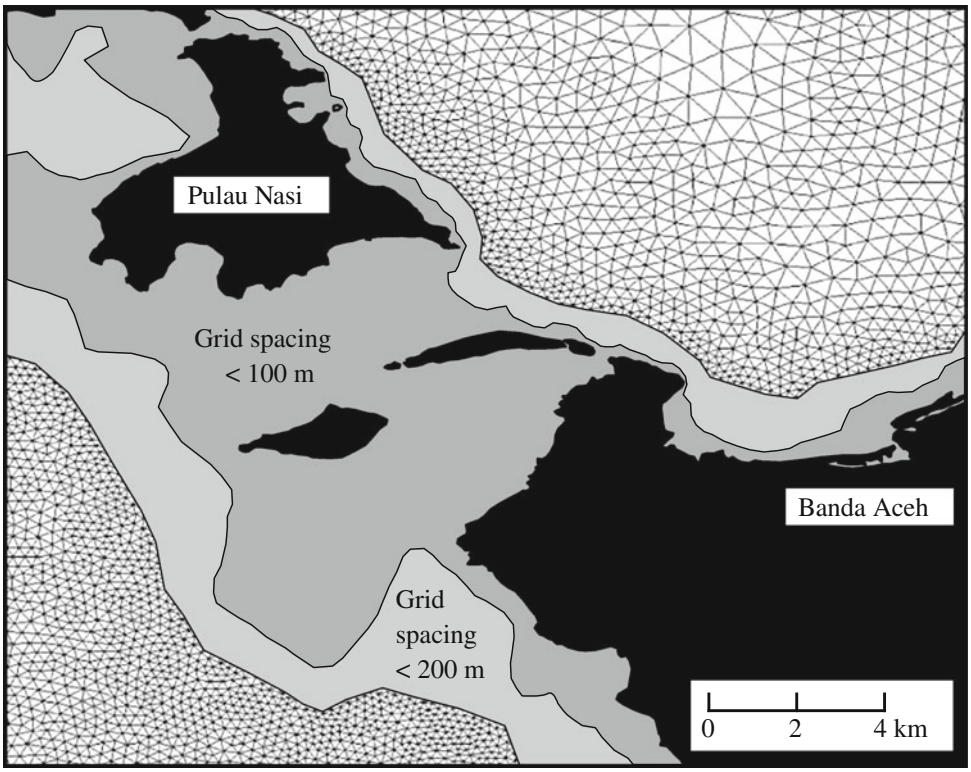

Fig. 2.6 Unstructured, variable grid of bathymetry around Banda Aceh, Indonesia used to simulate the effects of the Indian Ocean Tsunami of December 26, Based on Harig et al. (2008)

is now possible to provide real time simulations of most tsunami simply by matching an event to one in a database.

2.5 Run-Up and Inundation

2.5.1 Run-Up

Tsunami are known for their dramatic run-up heights, which commonly are greater than the height of the tsunami approaching shore by a factor of 2 or more times. The National Geophysical Data Center (2013) catalogue lists 32 events with a run-up of 30 m or more. For example, in the Pacific Ocean region, 44 tsunami have generated wave run-up heights in excess of 10 m since 1900. The largest run-up produced by a volcano was 90 m on August 29, 1741 on the west coasts of Oshima and Hokkaido Islands, Japan. The eruption of Krakatau in 1883 generated a wave that reached elevations up to 40 m high along the surrounding coastline (Blong 1984). The largest tsunami run-up generated by an earthquake was 100 m on Ambon Island, Indonesia, on February 17, 1674. In recent times, the tsunami that struck Flores Island on December 12, 1992 had a run-up of 26.2 m at Riang–Kroko, the Alaskan Tsunami of April 1, 1946 overtopped cliffs on Unimak Island and wiped out a radio mast standing 35 m above sea level (Fig. 2.8), and the Tōhoku Tsunami of 2011 produced run-up of 38.9 m. By far the largest run-up height recorded was that produced on July 9, 1958 by an earthquake-triggered landslide in Lituya Bay, Alaska (Miller 1960). Water swept 524 m above sea level up the slope on the opposite side of the bay, and a 30–50 m high tsunami propagated down the bay.

Wind-generated waves are limited in Stokes wave theory by depth. A Stokes wave will break when the height-to-water depth ratio exceeds 0.78. Thus, on flat coasts storm waves break in a surf zone and dissipate most of their energy before reaching shore. On the other hand, 75 % of tsunami reach shore without breaking, bringing tremendous power to bear on the coastline, and surging landward at speeds of 5 s^{-1} –8 m s^{-1} (Fig. 2.9). The opposite occurs on steep coasts such as those dominated by rocky headlands. Here, storm waves surge onto shore without breaking, whereas a tsunami wave is more likely to break. The popular media often portray this latter aspect as a plunging tsunami wave breaking over the coast. Under tsunami waves, significant water motion occurs throughout the whole water column. Close to the coast, this aspect is best described by a solitary wave (Fig. 2.4) (Geist 1997). A solitary wave maintains its form into shallowing water, and, because the kinetic energy of the tsunami is evenly distributed throughout the water column, little energy is dissipated, especially on steep coasts. Synolakis (1987) approximated the maximum run-up height of a solitary wave using the following formula:

$$H_{rmax} = 2.83\,(\cot\beta)^{0.5} H_t^{1.25} \qquad (2.11)$$

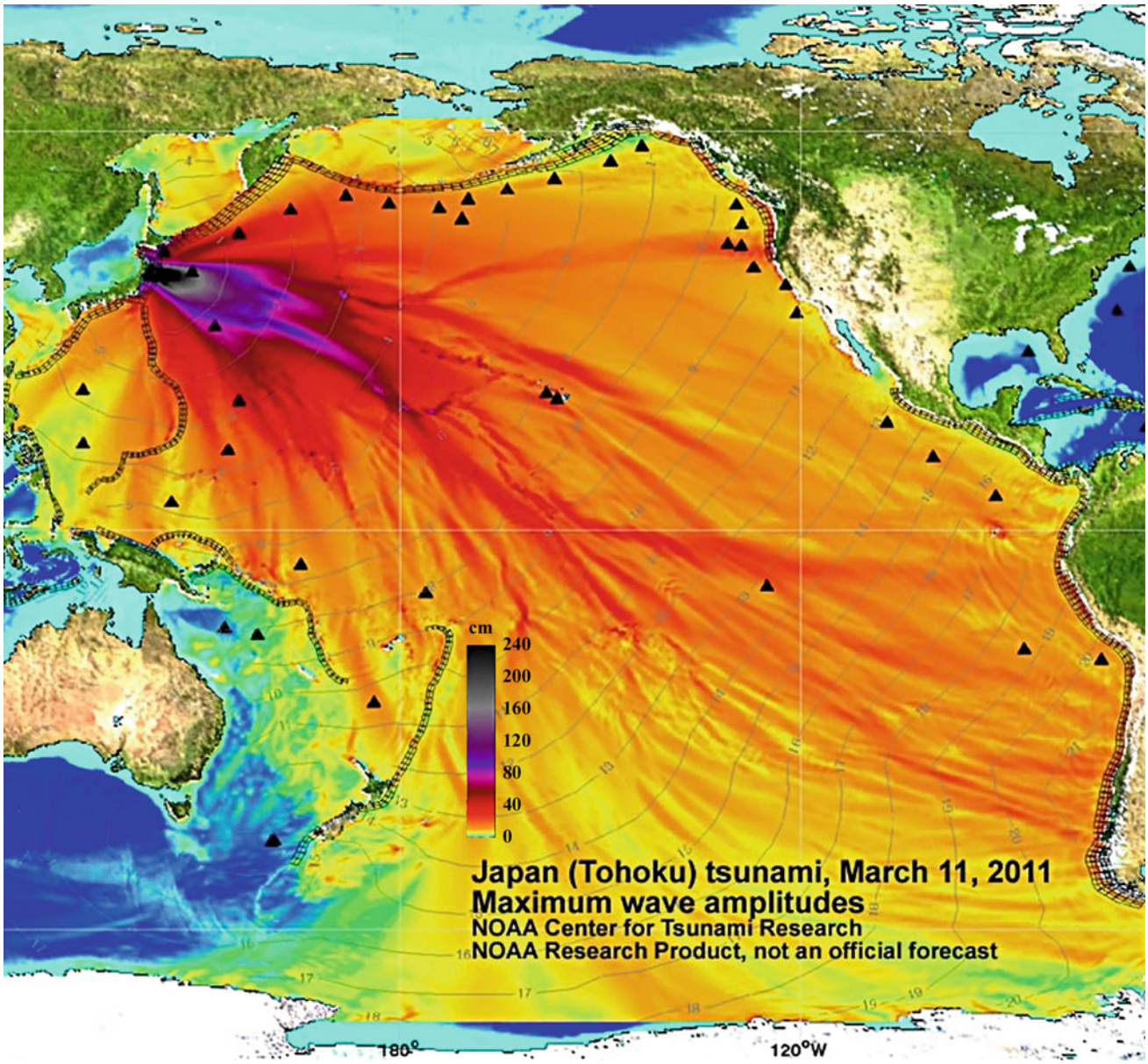

Fig. 2.7 Maximum wave heights for the Tōhoku Tsunami of March 11, 2011, simulated across the Pacific ocean using the MOST (Method of Splitting Tsunami) model. *Source* NOAA Center for Tsunami Research http://nctr.pmel.noaa.gov/honshu20110311/Energy_plot20110311_no_tg_lables_cropped_ok.jpg

where

H_{rmax} = maximum run-up height of a tsunami above sea level (m)
H_t = wave height at shore or the toe of a beach (m)
β = slope of the seabed (degrees)

The run-ups derived from Eq. 2.11 are higher than those predicted using sinusoidal waves. If a leading trough precedes the tsunami, then its form is best characterized by an *N*-wave (Fig. 2.4). These waves are more likely to be generated close to shore because the critical distance over which a tsunami wave develops is not long enough relative to the tsunami's wavelength to generate a wave with a leading crest. This critical distance may be as great as 100 km from shore—a value that encompasses many near-coastal tsunamigenic earthquakes. *N*-waves, as shown in Fig. 2.4 can take on two forms: simple and double (Geist 1997). The double wave is preceded by a smaller wave. The tsunami generated by the Indian Ocean Tsunami along the south Sri Lankan coast was a double *N*-wave. Tadepalli and

Fig. 2.8 The remains of the Scotch Cap lighthouse, Unimak island, Alaska, following the April 1, 1946 Tsunami. A coast guard station, situated at the top of the cliff 32 m above sea level, was also destroyed. Five men in the lighthouse at the time perished. *Source* United States Department of Commerce, National Geophysical Data Center

Synolakis (1994) approximated run-ups for *N*-waves using the following formulae:

$$\text{Simple } N\text{-wave} \quad H_{\text{rmax}} = 3.86\,(\cot\beta)^{0.5} H_t^{1.25} \qquad (2.12)$$

$$\text{Double } N\text{-wave} \quad H_{\text{rmax}} = 4.55\,(\cot\beta)^{0.5} H_t^{1.25} \qquad (2.13)$$

The two equations are similar in form to Eq. 2.11 for solitary waves. However, they result in run-ups that are 36 and 62 % higher. In some cases, *N*-waves may account for the large run-ups produced by small earthquakes. For example, an earthquake (M_s magnitude of 7.3) struck the island of Pentecost, Vanuatu, on November 26, 1999 (Caminade et al. 2000). Normally, an event of this magnitude would generate only a minor tsunami, if one at all. Instead, run-up reached 5 m above sea level. The tsunami was characterized by a distinct leading depression.

The run-up height of a tsunami also depends upon the configuration of the shore, diffraction, standing wave resonance, the generation of edge waves that run at right angles to the shoreline, the trapping of incident wave energy by refraction of reflected waves from the coast, and the formation of Mach–Stem waves (Wiegel 1964, 1970; Camfield 1994). Mach–Stem waves are not a well-recognized feature in coastal dynamics. They have their origin in the study of flow dynamics along the edge of airplane wings, where energy tends to accumulate at the boundary between the wing and air flowing past it. In the coastal zone, Mach–Stem waves develop wherever the angle between the wave crest and a cliff face is greater than 70°. The portion of the wave nearest the cliff continues to grow in amplitude even if the cliff line curves back from the ocean. The Mach–Stem wave process is insensitive to irregularities in the cliff face. It can increase ocean swell by a factor of four times. The process often accounts for fishermen being swept off rock platforms during rough seas. The process explains how cliffs 30 m or more in height can be overtopped by a shoaling tsunami wave that produces run-up reaching only one third as high elsewhere along the coast. Mach–Stem waves play a significant role in the generation of high-speed vortices responsible for bedrock sculpturing by large tsunami—a process that will be described in the following chapter.

All these processes, except Mach–Stem waves, are sensitive to changes in shoreline geometry. This variability accounts for the wide variation in tsunami wave heights over short distances. Within some embayments, it takes several waves to build up peak tsunami wave heights. Figure 2.10 maps the run-up heights around Hawaii for the Alaskan Tsunami of April 1, 1946 (Shepard 1977; Camfield 1994). The northern coastline facing the tsunami received the highest run-up. However, there was also a tendency for waves to wrap around the islands and reach higher run-ups at supposedly protected sites, especially on the islands of Kauai and Hawaii. Because of refraction effects, almost every promontory also experienced large run-ups, often more than

Fig. 2.9 Sequential photographs of the March 9, 1957 Tsunami overriding the backshore at Laie point on the island of Oahu, Hawaii. An earthquake in the Aleutian islands 3,600 km away, with a surface magnitude of 8.3, generated the tsunami. Photograph credit: Henry Helbush. *Source* United States Geological Survey, catalogue of disasters #B57C09-002

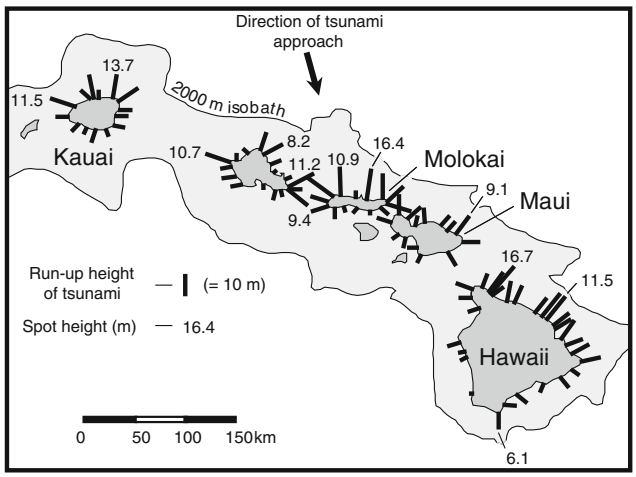

Fig. 2.10 Run-up heights around the Hawaiian islands for the Alaskan Tsunami of April 1, 1946. Based on Shepard (1977)

5 m high. Steep coastlines were hardest hit because the tsunami waves could approach shore with minimal energy dissipation. For all of these reasons, run-up heights were spatially very variable. In some places, for example on the north shore of Molokai, heights exceeded 10 m, while several kilometers away they did not exceed 2.5 m.

Tsunami interaction with inshore topography also explains why larger waves often appear later in a tsunami wave train. For example during the 1868 Tsunami off Arica, South America, the *USS Wateree* and the Peruvian ship *America* escaped the first two waves, but were picked up by a third wave 21 m high (Camfield 1994). The wave moved the two ships 5 km up the coast and 3 km inland, overtopping sand dunes (Fig. 2.11). The ships came to rest at the foot of the coastal range, where run-up had surged to a height 14 m above sea level. Similarly, during the April 1, 1946 Tsunami that devastated Hilo, Hawaii (the same tsunami that destroyed the Scotch Cap lighthouse shown in Figs. 2.1 and 2.9), many people were killed by the third wave, which was much higher than the preceding two.

Shallow-water long-wave equations can accurately simulate run-up. Figure 2.12 presents the results for a tsunami originally 3 m high with a period of 900 s traveling across a shelf of 12 m depth onto a beach of 1 % slope (Mader 1990). Under these conditions, linear theory would have the wave breaking several kilometers from shore. However, the shallow-water long-wave equations indicate that the wave surges onto the beach with a wave front that is 3.5 m high. This is similar to many descriptions of tsunami approaching shallow coasts, especially the one that approached the coast of Thailand during the Indian Ocean Tsunami event. While flooding can occur long distances inland, the velocity of the wave front can slow dramatically. During the Oaxaca, Mexico Tsunami of October 9, 1995, people were able to outrun the wave as it progressed inland (Anon 2005). A tsunami's backwash can be just as fast as, if not faster than, its run-up. The modeled wave shown in Fig. 2.12 took 300 s to reach its most shoreward point, but just over 100 s to retreat from the coast. Tsunami backwash is potentially just as dangerous as run-up. Unfortunately, little work has been done on tsunami backwash.

The sheltered locations on the lee side of islands appear particularly vulnerable to tsunami run-up (Briggs et al. 1995). Solitary waves propagate easily along steep shores, forming a trapped edge wave. Laboratory models show that the maximum run-up height of this trapped wave is greatest towards the rear of an island. More importantly, the run-up velocity here can be up to three times faster than at the front. For example, the December 12, 1992 tsunami along the north coast of Flores Island, Indonesia, devastated two villages in the lee of Babi, a small coastal island lying 5 km offshore (Yeh et al. 1993, 1994; Tsuji et al. 1995). Run-up having maximum heights of 5.6–7.1 m completely destroyed two villages and killed 2,200 people. Similarly, during the July 12, 1993 Tsunami in the Sea of Japan, the town of Hamatsumae, lying behind the Island of Okusihir, was destroyed by a 30 m high tsunami run-up that killed 330 people (Shuto and Matsutomi 1995).

Finally, tsunami run-up can also take on complex forms. Video images of tsunami waves approaching shore show that some decay into one or more bores. A bore is a special waveform in which the mass of water propagates shoreward with the wave (Yeh 1991). The leading edge of the wave is often turbulent. Waves in very shallow water can also break down into multiple bores or solitons. Soliton formation can be witnessed on many beaches where wind-generated waves cross a shallow shoal, particularly at low tide. Such waves are paradoxical because bores should dissipate their energy rapidly through turbulence and frictional attenuation, especially on dry land. However, tsunami bores are particularly damaging as they cross a shoreline. Detailed analysis indicates that the bore pushes a small wedge-shaped body of water shoreward as it approaches the shoreline. This transfers momentum to the wedge, increasing water velocity and turbulence by a factor of two. While there is a rapid decrease in velocity inland, material in the zone of turbulence can be subject to impact forces greater than those produced by ordinary waves. Often objects can travel so fast that they become water-borne missiles. This process can also transport a large amount of beach sediment inland. Tsunami that degenerate into bores are thus particularly effective in sweeping debris inland. Bores were crucial in the way the Indian Ocean Tsunami of 2004 impacted the west coast of Thailand and the Tōhoku Tsunami of 2011 propagated across the Sendai Plain.

Fig. 2.11 The American warship Wateree in the foreground and the Peruvian warship America in the background. Both ships were carried inland 3 km by a 21 m high tsunami wave during the Arica, South American event of August 13, 1868. Retreat of the sea from the coast preceded the wave, bottoming both boats. The Wateree, being flat hulled, bottomed upright and then surfed the crest of the tsunami wave. The America, being keel-shaped, was rolled repeatedly by the tsunami. Photograph courtesy of the United States Geological Survey. *Source* Catalogue of Disasters #A68H08-002

2.5.2 Inland Penetration and Velocity

As a rough rule of thumb, the cross-sectional area of coastline flooded by a tsunami is equal to the cross-sectional area of water under the wave crest close to shore (Fig. 2.13). The bigger the tsunami, or the longer its wave period, the greater the volume of water carried onshore and the greater the extent of flooding. The maximum distance that run-up can penetrate inland on flat and sloping coasts can be calculated using the following formulae (Hills and Mader 1997; Pignatelli et al. 2009):

$$x_{\max} = (H_t)^{1.33} n^{-2} k \tag{2.14}$$

$$x_{\max} = (H_t)^{1.33} n^{-2} k \cos \beta_l \tag{2.15}$$

where

$x_{\max}$ = limit of landward incursion (m)
n = Manning's n
k = a constant
β_l = slope of land surface

Very smooth terrain such as mud flats or pastures has a Manning's n of 0.015. Areas covered in buildings have a value of 0.03, and densely treed landscapes have a value of 0.07. The constant, k, in Eq. 2.14 has been evaluated for many tsunami and has a value of 0.06. The equation assumes that the run-up height equals the maximum depth of the tsunami at shore. Using this value, the maximum distance that tsunami can flood inland is plotted in Fig. 2.14 for different run-up heights, for the three values of

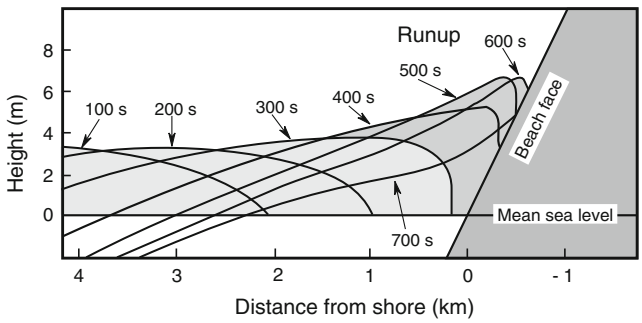

Fig. 2.12 Run-up of a tsunami wave onto a beach modeled using shallow-water, long-wave equations. The model used a grid spacing of 10 m and 0.5 s time increments. The original sinusoidal wave had a height of 3 m and a period of 900 s. Run-up peaked at 6 m above mean sea level and penetrated 600 m inland on a 1 % slope. Based on Mader (1990)

Manning's n mentioned. For developed land on flat coastal plains, a tsunami with a height of 10 m at shore can penetrate 1.4 km inland. Exceptional tsunami with heights at shore of 40–50 m can race 9–12 km inland. Only large earthquakes, submarine landslides, and asteroid impacts with the ocean can generate these latter wave heights. For crops or pasture, the same waves could theoretically rush inland four times further—distances of 5.8 km for a 10 m high wave at shore and 36–49 km for the 40–50 m high tsunami. The Indian Ocean Tsunami at Banda Aceh, Indonesia in 2004 with a height of 10 m at shore reached these predicted limits, traveling 5 km inland. Equation 2.14, and field research (Shuto 1993), also indicates that the effect of

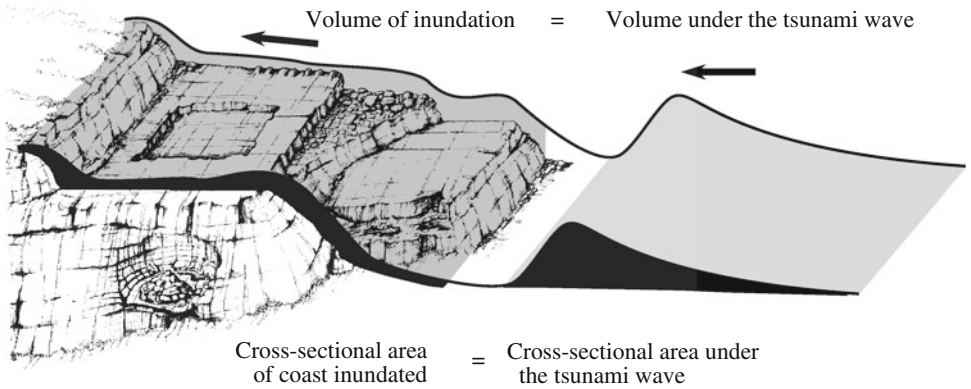

Fig. 2.13 Schematic diagram showing that the cross-sectional area of coastline flooded, and volume of inundation by a tsunami is equal to the cross-sectional area and volume of water under the tsunami wave crest. The landscape represented in this diagram will be described in Chap. 4

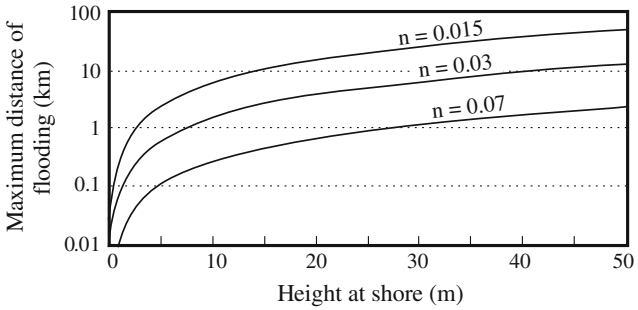

Fig. 2.14 Tsunami height versus landward limit of flooding on a flat coastal plain of varying roughness. Roughness is represented by Manning's n, where n equals 0.015 for very smooth topography, 0.03 for developed land, and 0.07 for a densely treed landscape. Based on Hills and Mader (1997)

a tsunami can be minimized on flat coastal plains by planting dense stands of trees. For example, a 10 m high tsunami can only penetrate 260 m inland across a forested coastal plain where the trees have a diameter large enough to withstand the high flow velocities without snapping.

Equation 2.2 indicates that the velocity of a tsunami wave is solely a function of water depth. Once a tsunami wave reaches dry land, wave height equates with water depth and the following equations apply:

$$H_t = d \tag{2.16}$$

$$v_r = 2(gH_t)^{0.5} \tag{2.17}$$

where

v_r = velocity of run-up (m s^{-1})
d = the depth of water flow over land (m)

This equation yields velocities of 8 s^{-1}– 9 m s^{-1} for a 2 m high tsunami wave at shore (Camfield 1994). Where tsunami behave as solitary waves and encircle steep islands, velocities in the lee of the island have been found to be three times higher than those calculated using this equation (Yeh et al. 1994). The velocity defined by Eq. 2.17 has the potential to move sediment and erode bedrock, producing geomorphic features in the coastal landscape that uniquely define the present of both present-day and past tsunami events. These signatures will be described in detail in the following chapter.

References

Anon., La Manzanillo Tsunami. University Southern California Tsunami Research Group website (2005), http://www.usc.edu/dept/tsunamis/manzanillo/

R.J. Blong, *Volcanic Hazards: A Sourcebook on the Effects of Eruptions* (Academic Press, Sydney, 1984)

B.A. Bolt, W.L. Horn, G.A. MacDonald, R.F. Scott, *Geological Hazards* (Springer, Berlin, 1975)

M.J. Briggs, C.E. Synolakis, G.S. Harkins, D.R. Green, Laboratory experiments of tsunami runup on a circular island. Pure. appl. Geophys. **144**, 569–593 (1995)

E. Bryant, *Natural Hazards*, 2nd edn. (Cambridge University Press, Cambridge, 2005)

J.P. Caminade, D. Charlie, U. Kanoglu, S. Koshimura, H. Matsutomi, A. Moore, C. Ruscher, C. Synolakis, T. Takahashi, Vanuatu earthquake and tsunami cause much damage, few casualties. Eos Trans. Am. Geophys. Union **81**(641), 646–647 (2000)

F.E. Camfield, Tsunami effects on coastal structures. J.Coastal Res. Spec. Issue No. 2, 177–187 (1994)

B.H. Choi, E. Pelinovsky, K.O. Kim, J.S. Lee, Simulation of the trans-oceanic tsunami propagation due to the 1883 Krakatau volcanic eruption. Nat. Hazards Earth Syst. Sci. **3**, 321–332 (2003)

E.L. Geist, Local tsunamis and earthquake source parameters. Adv. Geophys. **39**, 117–209 (1997)

S. Harig, C. Chaeroni, W.S. Pranowo, J. Behrens, Tsunami simulations on several scales. Ocean Dyn. **58**, 429–440 (2008)

J.G. Hills, C.L. Mader, Tsunami produced by the impacts of small asteroids. Ann. N. Y. Acad. Sci. **822**, 381–394 (1997)

F. Imamura, A.C. Yalciner, G. Ozyurt, Tsunami modelling manual (TUNAMI model) (2006), http://www.tsunami.civil.tohoku.ac.jp/hokusai3/E/projects/manual-ver-3.1.pdf

K. Iida, T. Iwasaki (eds.), *Tsunamis: Their Science and Engineering* (Reidel, Dordrecht, 1983)

P.D. Komar, *Beach Processes and Sedimentation*, 2nd edn. (Prentice-Hall, Upper Saddle River, 1998)
P.L.F. Liu, H. Yeh, C. Synolakis (eds.), *Advanced Numerical Models for Simulating Tsunami Waves and Runup* (World Scientific Publishing Company, Singapore, 2008)
C.L. Mader, Numerical simulation of tsunamis. J. Phys. Oceanogr. **4**, 74–82 (1974)
C.L. Mader, *Numerical modeling of water waves* (University of California Press, Berkeley, 1988)
C.L. Mader, Numerical tsunami flooding study: 1. Sci. Tsunami Hazards **8**, 79–96 (1990)
D.J. Miller, Giant waves in Lituya Bay, Alaska. US Geol. Surv. Prof. Pap. **354-C**, 51–86 (1960)
S. Murata, F. Imamura, K. Katoh, Y. Kawata, S. Takahashi, T. Takayama, Tsunami: To survive from Tsunami. Advance Series on Ocean Engineering 32, (Kindle edition) (World Scientific, New Jersey, 2010)
D. Myles, *The Great Waves* (McGraw-Hill, New York, 1985)
National Geophysical Data Center 2013. (NGDC/WDS) Global Historical Tsunami Database. Boulder, Colorado. http://www.ngdc.noaa.gov/hazard/tsu_db.shtml
E.A. Okal, Seismic parameters controlling far-field tsunami amplitudes: a review. Nat. Hazards **1**, 67–96 (1988)
E. Pelinovsky, *Tsunami Wave Hydrodynamics* (Institute of Applied Physics, Nizhny Novgorod, 1996). (in Russian)
C. Pignatelli, G. Sansò, G. Mastronuzzi, Evaluation of tsunami flooding using geomorphologic evidence. Mar. Geol. **260**, 6–18 (2009)
F.P. Shepard, *Geological Oceanography* (University of Queensland Press, St. Lucia, 1977)
N. Shuto, Tsunami intensity and disasters, in *Tsunamis in the World*, ed. by S. Tinti (Kluwer, Dordrecht, 1993), pp. 197–216
N. Shuto, H. Matsutomi, Field Survey of the 1993 Hokkaido Nansei-Oki earthquake tsunami. Pure. appl. Geophys. **144**, 649–663 (1995)
C.E. Synolakis, The run-up of solitary waves. J. Fluid Mech. **185**, 523–545 (1987)
C.E. Synolakis, E.N. Bernard, V.V. Titov, U. Kânoğlu, F.I. González, Validation and verification of Tsunami numerical models. Pure Appl. Geophys. **165**, 2197–2228 (2008)
S. Tadepalli, C.E. Synolakis, The run-up of N-waves on sloping beaches. Proc. R. Soc. Lond. **A445**, 111–112 (1994)
A.S. Trenhaile, *Coastal Dynamics and Landforms* (Oxford University Press, Oxford, 1997)
Y. Tsuji, H. Matsutomi, F. Imamura, M. Takeo, Y. Kawata, M. Matsuyama, T. Takahashi, Sunarjo, P. Harjadi, Damage to coastal villages due to the 1992 Flores Island earthquake tsunami. Pure Appl. Geophys. **144**, 481–524 (1995)
V.V. Titov, F.I. González, Implementation and testing of the method of splitting tsunami (MOST) Model. NOAA Technical Memorandum ERL PMEL No. 112 (1997), http://www.pmel.noaa.gov/pubs/PDF/tito1927/tito1927.pdf
H.C. von Baeyer, Catch the wave. The Sciences **29**, 10–13 (1999)
R.L. Wiegel, *Oceanographical Engineering* (Prentice-Hall, Englewood Cliffs, 1964), pp. 95–108
R.L. Wiegel, Tsunamis, in *Earthquake Engineering*, ed. by R.L. Wiegel (Prentice-Hall, Englewood Cliffs, 1970), pp. 253–306
H.H. Yeh, Tsunami bore runup. Nat. Hazards **4**, 209–220 (1991)
H.H. Yeh, P. Liu, M. Briggs, C. Synolakis, Propagation and amplification of tsunamis at coastal boundaries. Nature **372**, 353–355 (1994)
H.H. Yeh, F. Imamura, C. Synolakis, Y. Tsuji, P. Liu, S. Shi, The Flores Island tsunamis. EOS Trans. Am. Geophys. Union **74**, 369.S (1993)
Y.J. Zhang, A.M. Baptista, An efficient and robust tsunami model on unstructured grids. Part I: inundation benchmarks. Pure. appl. Geophys. **165**, 1–20 (2008)

http://www.springer.com/978-3-319-06132-0

Tsunami
The Underrated Hazard
Bryant, E.
2014, XXXI, 222 p. 149 illus., 8 illus. in color., Hardcover
ISBN: 978-3-319-06132-0